

OPEN

## profiling analysis of duodenum transcriptomes in SD rats administered ferrous sulfate or ferrous glycine chelate by gavage

A

Zhao Zhuo, Shenglin

Hu

Huan

The absorption of different iron sources is a trending research topic. Many studies have revealed that organic iron exhibits better bioavailability than inorganic iron, but the concrete underlying mechanism is still unclear. In the present study, we examined the differences in bioavailability of ferrous sulfate and ferrous glycinate in the intestines of SD rats using Illumina sequencing technology. Digital gene expression analysis resulted in the generation of almost 128 million clean reads, with expression data for 17,089 unigenes. A total of 123 differentially expressed genes with a  $|\log_2(\text{fold change})| > 1$  and  $\text{q-value} < 0.05$  were identified between the  $\text{FeSO}_4$  and Fe-Gly groups. Gene Ontology functional analysis revealed that these genes were involved in oxidoreductase activity, iron ion binding, and heme binding. Kyoto Encyclopedia of Genes and Genomes pathway analysis also showed relevant important pathways. In addition, the expression patterns of 9 randomly selected genes were further validated by qRT-PCR, which confirmed the digital gene expression results. Our study showed that the two iron sources might share the same absorption mechanism, and that differences in bioavailability between  $\text{FeSO}_4$  and Fe-Gly were not only in the absorption process but also during the transport and utilization process.

Iron is an essential trace element for life that is involved in various biologic processes, including oxygen transport, energy metabolism, DNA biosynthesis and oxidative phosphorylation<sup>1,2</sup>. It lacks a controlled excretion mechanism; therefore, iron homeostasis in the body is primarily regulated by iron absorption from the duodenal epithelium and its recycling in macrophages and other tissue stores<sup>3,4</sup>. Iron is potentially toxic, and its accumulation in the body results in the generation of reactive oxygen species (ROS)<sup>5,6</sup>. However, iron deficiency is a prevalent nutritional problem affecting humans and animals<sup>7</sup>. Dietary iron supplementation has long been used to prevent and treat iron deficiency in animals<sup>8,9</sup>, but different iron sources vary in their bioavailability.

It has been reported that iron chelated with amino acid or protein has good bioavailability in animals<sup>10–12</sup>. Recent studies have shown that ferrous glycinate (Fe-Gly) is more effective in animal production than ferrous sulfate ( $\text{FeSO}_4$ )<sup>13,14</sup>. Fe-Gly is absorbed more efficiently and utilized faster than  $\text{FeSO}_4$ , and in addition, the expression of intestinal transport proteins differs in the presence of these two iron sources<sup>15</sup>. However, the concrete mechanism underlying the absorption of these two iron sources is still unknown.

Next generation sequencing (NGS) techniques are effective methods that have dramatically improved the speed and efficiency of the identification of novel genes<sup>16,17</sup>. Digital gene expression (DGE), a tag-based transcriptome sequencing method, is one such technique that can be applied to analyze quantitative gene expression and to compare expression profiles without being affected by potential bias, thereby enabling sensitive and accurate transcriptome profiling<sup>18,19</sup>.

In this study, we applied RNA sequencing technology to assess the absorption mechanisms of different iron sources in the intestines of Sprague-Dawley (SD) rats. Because iron is mainly absorbed in the duodenum<sup>20,21</sup>, only

Key Laboratory of Molecular Animal Nutrition, Ministry of Education, College of Animal Science, Zhejiang University,

Age in Weeks	Body Weight	
	FeSO <sub>4</sub>	Fe-Gly
4 w	81.5 ± 5.82	79.7 ± 7.76
6 w	191.7 ± 4.04	193.2 ± 10.34

**Table 1.** The body weights of the SD rats at 4 and 6 weeks of age. The values are presented as the mean ± standard deviation (n = 12).

Parameter	Unit	FeSO <sub>4</sub>	Fe-Gly
WBC	10 <sup>9</sup> /L	4.5 ± 0.95	4.7 ± 1.34
RBC	10 <sup>12</sup> /L	5.8 ± 0.72	5.9 ± 0.39
Hb	g/L	120.0 ± 15.72	124.7 ± 7.12
HCT	%	35.9 ± 4.93	37.1 ± 2.05
MCV	fL	61.7 ± 1.16	63.3 ± 1.75
MCH	pg	20.7 ± 0.58	21.3 ± 0.82
MCHC	g/L	335.0 ± 7.00	336.0 ± 11.78

**Table 2.** Hematological parameters in the FeSO<sub>4</sub> and Fe-Gly group rats. Blood cell indices were determined for twelve SD rats in each group. White Blood Cell Count (WBC), Red Blood Cell Count (RBC), Hemoglobin Concentration (Hb), Hematocrit (HCT), Mean Corpuscular Volume (MCV), Mean Corpuscular Hemoglobin (MCH), and Mean Corpuscular Hemoglobin Concentration (MCHC). The values are presented as the mean ± standard deviation (n = 12).

Parameter	Unit	FeSO <sub>4</sub>	Fe-Gly
TIBC	μmol/L	103.6 ± 14.23	99.1 ± 14.66
SI	μmol/L	45.7 ± 5.12	66.7 ± 12.72*
TAST	%	45 ± 11.3	67 ± 9.0*

**Table 3.** Serum iron-related parameters in the SD rats. Total Iron Banding Capacity (TIBC), Serum Iron (SI), and Transferrin Saturation (TAST). The values are presented as the mean ± standard deviation (n = 12).

\*Indicates a significant difference in the mean value between the two groups at P < 0.05.

duodenal samples were examined in DGE analysis. By assembling and annotating the transcriptome sequences identified in these samples, and analyzing their gene expression profiles, we were able to identify differentially expressed genes in response to the two iron sources. The results of our DGE analysis have provided preliminary information regarding the differences between FeSO<sub>4</sub> and Fe-Gly absorption in SD rats.

## Results

**Iron status of SD rats.** After two weeks of treatment of the SD rats by intragastric administration of the different iron sources, the animals' body weights did not differ between the FeSO<sub>4</sub> and Fe-Gly groups (Table 1). In addition, no differences in the hematological parameters were observed between the two groups (Table 2). The serum total iron binding capacity (TIBC) were similar between the groups, but the serum iron (SI) levels were significantly different (P-value < 0.05, Table 3). The Fe-Gly group exhibited a higher serum iron concentration than the FeSO<sub>4</sub> group; therefore, transferrin saturation (TAST) was also increased (P-value < 0.05). The immunohistochemical staining of ferritin in the liver also differed between the two groups (Fig. 1). The liver biopsies of the Fe-Gly group in different magnifications (50 μm and 25 μm) showed increased positive staining, indicating enhanced ferritin deposition in the liver. These results were confirmed by calculation of the mean density (P-value < 0.05).

**Analysis of DGE libraries.** To detect differences in absorption between FeSO<sub>4</sub> and Fe-Gly, RNA-seq of duodenal samples was performed using the Illumina sequencing platform. Three individual samples were included for each group, and they were marked as C1, C2, and C3 and T1, T2, and T3, respectively. The main characteristics of the six libraries are summarized in Table 4. The C1, C2, C3, T1, T2, and T3 libraries contained 20,446,968, 20,983,958, 23,325,694, 21,951,812, 21,586,433, and 22,458,258 raw reads, respectively. After removing adaptor, ambiguous and low-quality sequences, 19,720,103, 20,414,770, 22,897,985, 21,550,142, 21,172,114, and 22,056,148 clean reads were remained. The percentage of clean reads among raw reads was greater than 96%.

**Mapping reads to the transcriptome.** For gene expression profiling, the sequencing reads from the six libraries were aligned to a reference database, which consisted of the *Rattus norvegicus* genome, using TopHat v2.0.9. More than 95% of the clean reads mapped to this database (Table 5). In particular, 17,935,148 (90.95%), 18,282,777 (89.56%), 20,841,830 (91.02%), 19,627,268 (91.08%), 19,087,487 (90.15%), and 19,997,125 (90.66%) reads from the C1, C2, C3, T1, T2, and T3 libraries, respectively, uniquely mapped to the reference database.

**Analysis of differential gene expression.** For analysis of gene expression, the number of unambiguous clean tags for each gene was calculated and normalized to the RPKM value. To increase the accuracy of the measured expression levels for further analyses, data from three biological replicates were merged, and RPKM values were calculated based on the merged dataset (ref. Table S1). To identify differentially expressed genes, a  $|\log_2(\text{fold change})| > 1$  and  $\text{q-value} < 0.05$  were used as standards. A volcano plot was generated to visualize the distribution of expressed genes between the groups (Fig. 2), and the red dots in this plot represent differentially expressed genes. The distribution of differentially expressed genes is depicted in the heatmap shown in Fig. 3. There were 123 differentially expressed genes in total, including 83 up-regulated and 40 down-regulated genes (ref. Table S2).

**Functional analysis of differentially expressed genes.** The differentially expressed genes were considered to be associated with changes in physiological function in the body. According to the Gene Ontology (GO) classification system, the 123 differentially expressed genes were classified into three main functional categories: biological process, cellular component and molecular function (ref. Table S3). Genes involved in the response to stimulus, metabolic process, response to chemical stimulus, and response to organic substance were predominant in the biological process category. In addition, plasma membrane, endomembrane system, membrane fraction and microsome were the predominant enriched terms in the cell components category. Moreover, a significant proportion of the genes were enriched in v7.4.5(l)4.5(v)8.5(e)-4.5(m)0.5(i)0.5(e)0.5(j)0.6(b)0.12 in hvcl cataltl ctlcocy, re cotoe ohvcl and

Taath

Item	C1	C2	C3	T1	T2	T3
Raw reads	20,446,968 (100%)	20,983,958 (100%)	23,325,694 (100%)	21,951,812 (100%)	21,586,433 (100%)	22,458,258 (100%)
adaptor sequences	385,382 (1.88%)	167,806 (0.80%)	22,261 (0.10%)	16,393 (0.07%)	19,553 (0.09%)	6,456 (0.03%)
ambiguous sequences	797 (<0.01%)	873 (<0.01%)	1,000 (<0.01%)	939 (<0.01%)	880 (<0.01%)	997 (<0.01%)
low-quality sequences	340,686 (1.67%)	400,509 (1.91%)	404,448 (1.73%)	384,338 (1.75%)	393,886 (1.82%)	394,657 (1.76%)
Clean reads	19,720,103 (96.45%)	20,414,770 (97.29%)	22,897,985 (98.17%)	21,550,142 (98.17%)	21,172,114 (98.08%)	22,056,148 (98.21%)
clean_Q20	98.95%	98.93%	98.96%	98.95%	98.92%	98.95%
clean_Q30	95.53%	95.42%	95.55%	95.53%	95.38%	95.52%

**Table 4.** Summary of sequencing analysis. C1, C2, and C3: control group, namely the FeSO<sub>4</sub> group; T1, T2, and T3: treatment group, namely the Fe-Gly group. Q20: the percentage of bases with a Phred value > 20; and Q30: the percentage of bases with a Phred value > 30.

Mapping Statistics	C1	C2	C3	T1	T2	T3
Effective reads	19,720,103 (100%)	20,414,770 (100%)	22,897,985 (100%)	21,550,142 (100%)	21,172,114 (100%)	22,056,148 (100%)
Total mapped	18,873,056 (95.70%)	19,518,820 (95.61%)	21,935,403 (95.80%)	20,668,869 (95.91%)	20,209,758 (95.45%)	21,191,619 (96.08%)
Multiple mapped	937,908 (4.76%)	1,236,043 (6.05%)	1,093,573 (4.78%)	1,041,601 (4.83%)	1,122,271 (5.30%)	1,194,494 (5.42%)
Uniquely mapped	17,935,148 (90.95%)	18,282,777 (89.56%)	20,841,830 (91.02%)	19,627,268 (91.08%)	19,087,487 (90.15%)	19,997,125 (90.66%)
Reads mapped to '+'	9,326,071 (47.29%)	9,611,103 (47.08%)	10,844,189 (47.36%)	10,227,148 (47.46%)	9,958,528 (47.04%)	10,452,084 (47.39%)
Reads mapped to '-'	9,546,985 (48.41%)	9,907,717 (48.53%)	11,091,214 (48.44%)	10,441,721 (48.45%)	10,251,230 (48.42%)	10,739,535 (48.69%)

**Table 5.** The data for the sequencing reads that mapped to the reference genome. C1, C2, and C3: control group, namely the FeSO<sub>4</sub> group; T1, T2, and T3: treatment group, namely the Fe-Gly group. “+” refers to the sense strand, and “-” refers to the anti-sense strand.

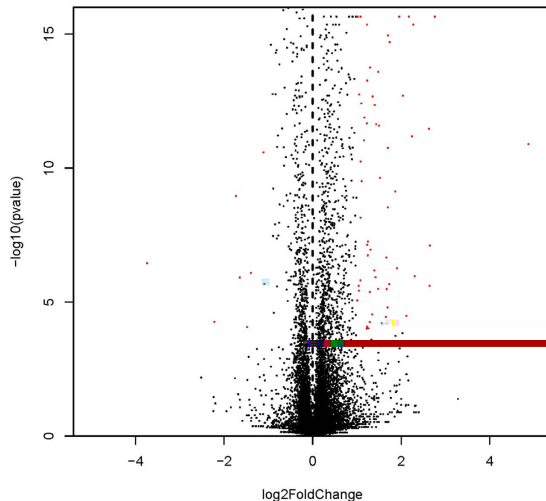


**Figure 2.** Volcano plot of differentially expressed genes. The abscissa represents the fold changes in gene expression, which were calculated as Fe-Gly (mean)/FeSO<sub>4</sub> (mean); the “mean” is the mean of three biological replicates. The ordinate represents the statistical significance of the variations in gene expression. The red dots represent significantly differentially expressed genes.

similar between the two groups, but TAST was significantly increased in the Fe-Gly group. These results suggested that more iron was transported into the bodies of the Fe-Gly-treated rats. However, administration of the two iron sources did not significantly influence the Hb level. This result is reasonable because the Hb level is usually within the normal range in humans and animals, and remains constant because it is regulated by the iron homeostasis system<sup>26</sup>. The liver is a reliable response criterion for the mineral status<sup>27</sup>, and ferritin is a protein that functions in iron storage *in vivo*<sup>28</sup>. The results showed increased positive staining for ferritin in the liver biopsies of the Fe-Gly group, suggesting that Fe-Gly was more easily absorbed and transported into the rats’ bodies than FeSO<sub>4</sub>.

To clarify the molecular mechanisms of FeSO<sub>4</sub> and Fe-Gly absorption, the transcriptomes of duodenal samples obtained from SD rats administered one of the two iron sources by gavage were sequenced using the Illumina platform. This approach provides a new method to study the absorption of different iron sources using the recently developed RNA-seq technology. In total, almost 128 million clean reads were obtained. Approximately 17,089

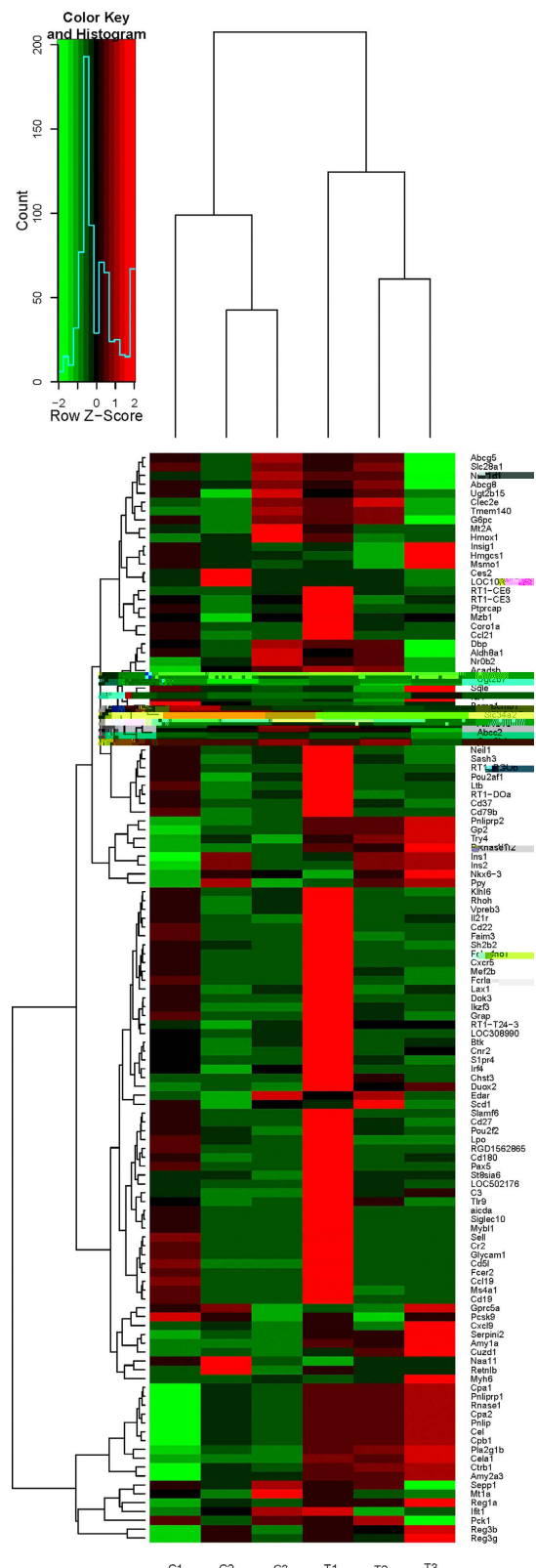


**Figure 3.** Heatmap of differentially expressed genes. C1, C2, and C3: control group, namely the  $\text{FeSO}_4$  group; T1, T2, and T3: treatment group, namely the Fe-Gly group.

unigenes were assembled, of which 100% were annotated (ref. Table S1). A total of 123 differentially expressed genes with a  $|\log_2(\text{fold change})| > 1$  and  $\text{q-value} < 0.05$  were identified between the  $\text{FeSO}_4$  and Fe-Gly groups.

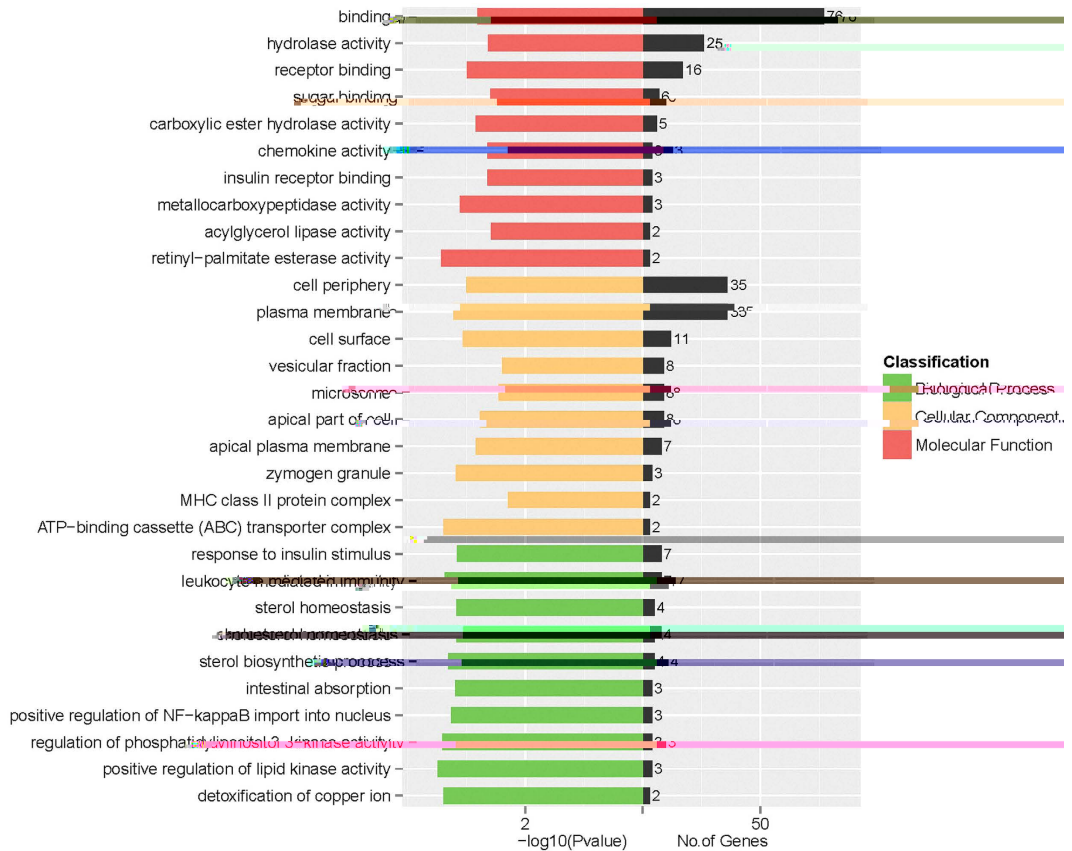


**Figure 4. GO functional enrichment analysis.** The differentially expressed genes between the FeSO<sub>4</sub> and Fe-Gly groups were classified based on Gene Ontology. Only a portion of the results are shown; for the complete dataset, please see ref. Table S3.

To validate the differentially expressed genes identified by RNA-seq, the expression levels of 9 genes were confirmed by qRT-PCR. Comparison of the results obtained using the two methods revealed similar trends of up-regulation and down-regulation.

According to the GO classifications, the differentially expressed genes were involved in oxidoreductase activity, iron ion binding, monooxygenase activity, and heme binding activity. Cyp2b1, Hmox1, Duox2, and Msmo1 were the main genes associated with these GO molecular function terms. In addition, KEGG pathway analysis of the 123 differentially expressed genes revealed that, metabolic pathways, pancreatic secretion, and cytokine-cytokine receptor interaction were the most highly enriched terms. We also focused on the differentially expressed genes related to the mineral absorption pathway, HIF-1 signaling pathway and ABC transporters.

A mineral absorption pathway was associated with a bunch of these elements absorption (e.g., for Ca, P, K, Na, Fe, Cu, Zn, Mn). They are one of the five fundamental groups of nutrients that clearly required for life, but most are quite toxic when present at higher than normal concentrations. Thus, there is a physiologic challenge of supporting efficient but limited absorption. In many cases intestinal absorption is a key regulatory step in mineral homeostasis. In the present study, three genes involved in the mineral absorption pathway were markedly up-regulated by Fe-Gly gavage, that are Hmox1, Mt1a and Mt2A. Heme oxygenase 1 (Hmox1) is involved in the release of iron from heme<sup>29</sup>. There are studies shown that rats cannot absorb heme iron as efficiently as humans do, and they don't require intestinal Hmox1 for dietary heme iron assimilation<sup>30,31</sup>. But glycine was one of the important substrate in the process of heme synthesis<sup>32</sup>, the increased Hmox1 expression of Fe-Gly group in our experiment indicated that Fe-Gly was more closely linked to intracellular heme metabolism than FeSO<sub>4</sub>. MTs are small (6–10 kDa), cysteine-rich (33%) metalloproteins that catalyze redox reactions and contain metal binding sites. Although they are mainly involved in the homeostasis of physiological Zn<sup>2+</sup>, they still exhibit the capacity to bind iron because they are thiolate-rich biomolecules<sup>33</sup>. Considering that the expression of Mt1a and Mt2A was significantly increased in the Fe-Gly group, we speculate that a much larger amount of iron was indeed absorbed into the intestinal epithelia of the rats in this group. Duodenal Npt 2b (Slc34a2) primarily mediates intestinal Pi absorption<sup>34</sup>, which was also the differentially expressed gene involved in the mineral absorption pathway. In our experiment, the down-regulated Slc34a2 by Fe-Gly gavage seem to indicate that the intracellular iron content will affect intestine Pi absorption.

As a master regulator of the hypoxia-signaling pathway, the HIF-1 signaling pathway has been conserved throughout evolution in species ranging from *Caenorhabditis elegans* to *Homo sapiens*, these pathways activate the expression of similar (or homogenous) genes, resulting in similar physical and biochemical responses,

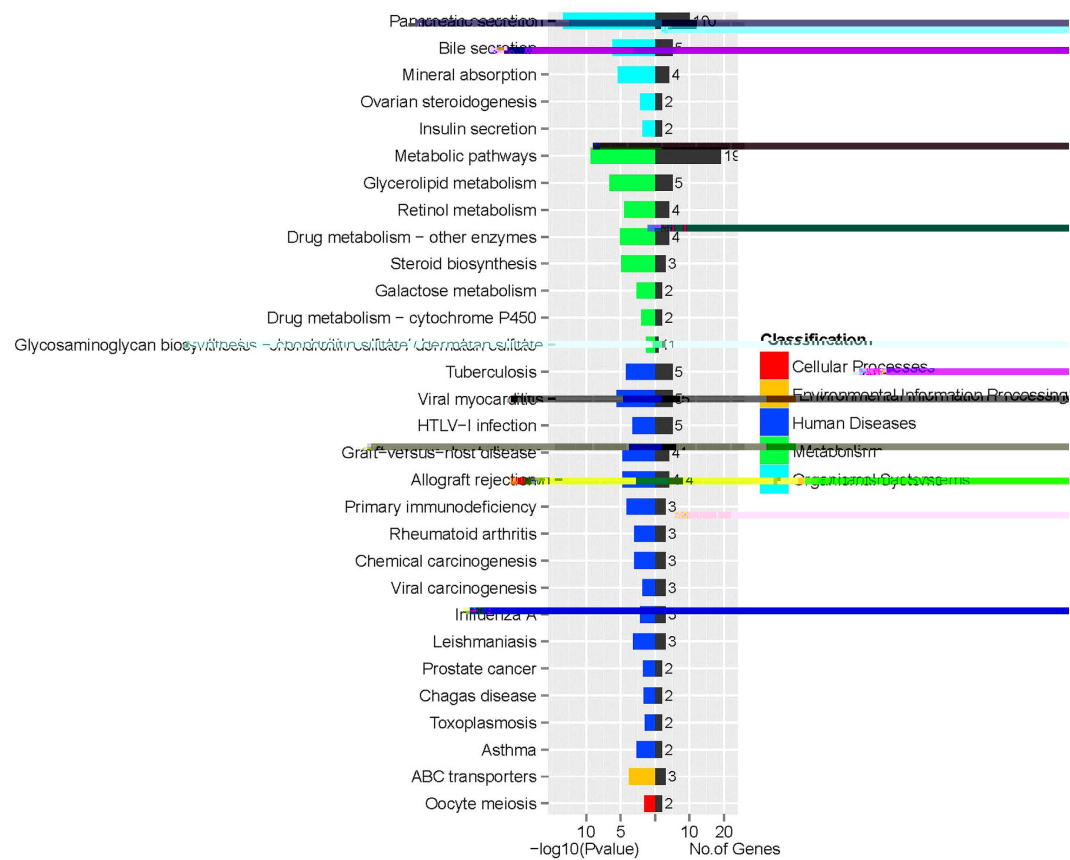


**Figure 5. KEGG pathway analysis.** The enriched pathways among the differentially expressed genes were identified by KEGG analysis. Only a portion of the results are shown; for the complete dataset, please see ref. Table S4.

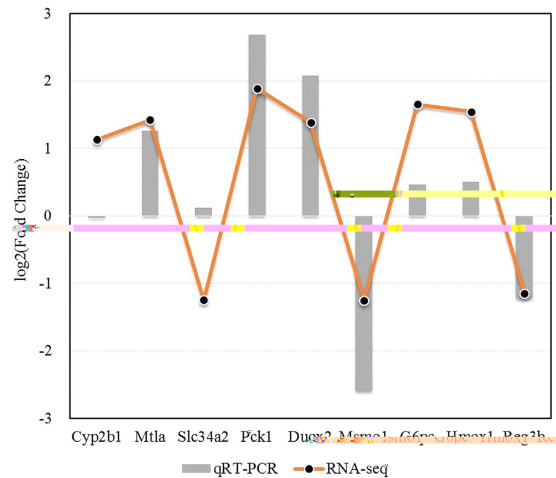


**Figure 6. Gene expression determined by RNA-seq and qRT-PCR.** qRT-PCR validation of nine differentially expressed genes between the FeSO<sub>4</sub> and Fe-Gly groups. The data were normalized to the expression of GAPDH, and the fold changes were calculated as Fe-Gly/FeSO<sub>4</sub>.

including oxygen sensing, oxygen transport, angiogenesis, erythropoiesis, and heme metabolism<sup>35</sup>. In this study, insulin 1 (Ins1) and insulin 2 (Ins2), which are involved in the HIF-1 signaling pathway, were down-regulated in the Fe-Gly group. Because the insulin level is increased under iron-deficient conditions<sup>36</sup>, it seems that the SD rats in the Fe-Gly group maintained better iron status than those in the FeSO<sub>4</sub> group.

ATP-binding cassette (ABC) transporters belong to one of the largest known protein families, and they are widespread in bacteria, archaea, and eukaryotes<sup>37</sup>. They couple ATP hydrolysis to the active transport of a wide

variety of substrates, such as ions, sugars, lipids, sterols, peptides, proteins, and drugs<sup>38</sup>. Heme and iron siderophores have been shown to be transported across the cytoplasmic membrane by ABC transporters<sup>39</sup>. In this study, three genes involved in the ABC transporter pathway were up-regulated in the Fe-Gly group, suggesting that Fe-Gly more effectively increased the activity of ABC transporters. Thus, the two iron sources may have had different fates after being absorbed by the intestinal epithelium.

To our knowledge, the intestinal absorption of inorganic iron often begins with the conversion of  $\text{Fe}^{3+}$  to  $\text{Fe}^{2+}$  by duodenal cytochrome b (DcytB), which is a membrane-associated ferrireductase<sup>40</sup>. Then, the reduced  $\text{Fe}^{2+}$  is transported across the apical membrane by divalent metal transporter 1 (DMT1/SLC11A2)<sup>41,42</sup>. The absorbed iron is either stored intracellularly for subsequent use or transported into the circulation by the only known iron export protein, ferroportin (FPN1/SLC40A1)<sup>43</sup>. We had previously thought that the difference in biological efficiency between  $\text{FeSO}_4$  and Fe-Gly might be attributed to their differing mechanisms of absorption. However, there were few differentially expressed genes related to iron metabolism between the two groups (Table 6).

Our previous cell experiments demonstrated that, in the same concentration,  $\text{FeSO}_4$  had more free iron ion than Fe-Gly<sup>44</sup>.  $\text{Fe}^{2+}$  is easily oxidized to be  $\text{Fe}^{3+}$ , and  $\text{Fe}^{3+}$  is apparently less effective in the body<sup>45,46</sup>. In addition, the environment of intestine is complex, many factors can affect iron absorption. Ferrous glycinate is a relatively stable compound, chelated with glycine ligand can protect iron from inhibitors in the intestine and keep it soluble and readily available<sup>47,48</sup>. Our results are more inclined to support that the two iron sources are absorbed through the inorganic iron way, their bioavailability differences might mainly due to difference in the absorption rate of iron in the intestine.

## Conclusion

In the present study, we examined the absorption differences between  $\text{FeSO}_4$  and Fe-Gly in SD rats. Digital gene expression profiling analysis based on Illumina sequencing technology provided comprehensive information on iron metabolism. There were 123 significantly differentially expressed genes in total, including 83 up-regulated and 40 down-regulated genes. GO functional analysis revealed that these genes were related to oxidoreductase activity, iron ion binding, and heme binding. KEGG pathway analysis showed that they were also involved in important pathway, such as mineral absorption, the HIF-1 signaling pathway and ABC transporters. In addition, the expression patterns of 9 genes were further validated by qRT-PCR, confirming the digital gene expression results. Our study indicated that the two iron sources might share the same absorption mechanism, and that  $\text{FeSO}_4$  and Fe-Gly might differ not only in their absorption process but also in their transport and utilization process.

## Methods

**Animals and experimental design.** All of the animal experiments were approved by the Animal Ethics Committee of Zhejiang University. The experimental procedures were performed in strict accordance with the Guidelines for the Care and Use of Laboratory Animals in China. This study was conducted at the Laboratory Animal Center of Zhejiang University. After two days of pre-feeding, twenty-four SD rats (males; 4 weeks old) were randomly assigned to receive one of the two treatments. Every day, the rats in each treatment group were perfused with 1 mL  $\text{FeSO}_4$  or Fe-Gly (80 mg/L as iron). The experiment lasted for two weeks.

The SD rats were reared in a clean standard room. Their diet was formulated according to the International Standards of Experimental Animals AIG-93G (purchased from Slack Experimental Animals LLC, Shanghai; for composition of the basal diet, see ref. Table S6). The temperature and relative humidity in the room were maintained at approximately 23–25 °C and 40–60%, respectively, with a twelve hour light/dark cycle. All of the rats were housed in stainless steel cages and were provided with deionized water to avoid the intake of extra iron.

**Sample collection and analysis.** The day before they were euthanized, the SD rats were fasted overnight with free access to deionized water. Then, the rats' body weights were recorded, and they were administered 1 mL  $\text{FeSO}_4$  or Fe-Gly at a relatively high dose (800 mg/L as iron). Two hours after gavage, the rats were anesthetized with chloral hydrate, and blood was collected from their eyeballs. The whole blood samples were sent to the Laboratory Animal Center of Zhejiang University for hematological measurements. Sera were separated by centrifugation at 3,000 × g for 10 min at 4 °C, and the iron levels were determined by using a serum iron assay kit (Jiancheng Bioengineering Institute, Nanjing, China).

Then, the rats were sacrificed by cervical dislocation, and liver specimens were obtained and fixed in 4% formaldehyde for immunohistochemical analysis. Approximately 3 cm of the duodenum was removed from each rat, washed with normal saline, and packed with sterile and RNase-free silver paper. After being rapidly frozen in liquid nitrogen, the samples were stored at –80 °C until RNA extraction.

**Immunohistochemical staining.** The liver tissues were fixed in 4% formaldehyde and embedded in paraffin. Immunohistochemical staining to detect ferritin was performed using a DAKO Envision System (DAKO Corporation) according to the manufacturer's protocol<sup>49</sup>.

Briefly, paraform-embedded liver tissues were cut into 5  $\mu\text{m}$  sections and placed on glass slides. The sections were deparaffinized with xylene, dehydrated with ethanol, and then incubated with 3% hydrogen peroxide to block endogenous peroxidase. Antigen retrieval was performed by heating the sections in 10 mM sodium citrate buffer (pH 6.0). Then, the sections were blocked with DAKO protein block (X9090; DAKO), followed by incubation with an FTL primary antibody (10727-1-AP; 1:100; Proteintech) overnight at 4 °C. Subsequently, they were incubated with the respective HRP-conjugated goat anti-rabbit (K4003; DAKO) secondary antibody for visualization of the target proteins. DAB reagent (K5007; DAKO) was applied for detection of these proteins. The tissue sections were counterstained with Aqua Hematoxylin-INNOVEX (Innovex Biosciences). Double immunohistochemistry was performed using Vina Green, according to the manufacturer's recommendations (BioCare Medical).

Metabolic process	Gene	Function	Illumina mRNA-seq (log2 fold change)
cellular iron/heme uptake	Tf	Plasma, lymph, and CSF ferric iron carrier	0.09
	Tfrc	Facilitates Tf-dependent iron uptake	-0.79
	Tfr2	Regulates hepcidin; mediates Tf-bound and non-transferrin-bound iron uptake	0.21
	Stear3	Erythroid endosomal ferrireductase	-0.08
	Slc11a2	Endosomal ferrous iron transporter; transmembrane non-transferrin iron transporter	0.15
	Cybrd1	Intestinal ferrireductase	0.21
	Slc39a4	Non-transferrin iron transporter in liver	0.38
	Tim2	H-ferritin receptor	0.28
	Scara5	L-ferritin receptor	0.18
	FLVCR2	Heme importer	0.70
	Slc46a1	Intestinal heme transporter	0.37
	Hmox1	Heme iron reutilization	1.55*
	Hmox2	Heme iron reutilization	0.10
	Lcn2	Facilitator of non-transferrin iron import	0.21
cellular iron storage	Fth1	Iron storage protein subunit; ferroxidase	0.11
	Ftl	Iron storage protein subunit	0.05
intracellular iron tracking	Fech	Insertion of iron into porphyrin	-0.12
	Alas2	Heme biogenesis	1.22
	Abcb10	Interacts with Fech and Mitoferrin-1; transport ligand unknown	-0.12
	Abcb7	Interacts with Fech; cytosolic ISC maturation	-0.01
	Abcb6	Import of porphyrin into mitochondria	0.24
	Slc25a37	Mitochondrial iron import	-0.08
	Bdh2	Siderophore biosynthesis	0.62
cellular iron/heme export	Abcg2	Partially exports heme; PPIX exporter	0.36
	Slc40a1	Regulates efflux of iron from cells	0.01
cellular iron balance	Aco1	Post-transcriptional regulation of target mRNAs via IREs; cytosolic aconitase	0.09
	Ireb2	Post-transcriptional regulation of target mRNAs via IREs	-0.12

**Table 6.** The main genes related to iron metabolism and their expression differences between the two groups. \*Indicates a significant difference in gene expression at  $q\text{-value} < 0.05$ . Fold change = Fe-Gly group (mean)/FeSO<sub>4</sub> group (mean); the “mean” is the mean of three biological replicates.

Liver specimens exposed to 1% bovine serum albumin instead of the respective primary antibody were used as negative controls. For the quantification of ferritin staining, 3 randomly chosen fields per section were evaluated at  $\times 200$  magnification for each sample. Image-Pro Plus 6.0 was used to determine integrated optical density (IOD) values, from which the mean density was calculated (IOD/AREA).

**RNA extraction and qualification.** Total RNA was isolated from the duodenal tissues using Trizol reagent (Invitrogen), according to the manufacturer’s protocol. RNA degradation and contamination were monitored using 1% agarose gels. RNA purity was assessed using an Nanodrop ND-1000 spectrophotometer (Thermo Scientific, USA). The A260:A280 and A260:A230 ratios of each RNA sample were above 1.8 and 2.0, respectively. RNA integrity was evaluated using an Agilent 2200 TapeStation (Agilent Technologies, USA) and each sample had an RINe value of above 7.0.

**Library preparation for DGE sequencing.** Three samples from each group were selected for digital gene expression measurements<sup>50</sup>. A total of 3  $\mu\text{g}$  RNA per sample was used as the input material for the sequencing. Briefly, mRNAs were isolated from total RNA and broken into fragments of approximately 200 bp in size. Subsequently, the collected mRNAs were subjected to first-strand and second-strand cDNA synthesis, followed by adaptor ligation and low-cycle enrichment, according to the instructions of a TruSeq®RNA LT/HT Sample Prep Kit (Illumina, USA). The purified products were evaluated using an Agilent 2200 TapeStation and Qubit®Q.0 (Life Technologies, USA). They were then diluted to 10 pM for cluster generation *in situ* on a HiSeq2500 pair-end flow cell, followed by sequencing ( $2 \times 100$  bp) with a HiSeq 2500 sequencer. All sequencing data were submitted to the NCBI database under accession number SRP075016.

**Quality control and mapping analyses.** Raw data (raw reads) in the FASTQ format were first processed using in-house Perl scripts. In this step, clean data were obtained by removing reads from the raw data that

contained adapter sequences and poly-N and those were low-quality. Then, the Q20, Q30 and GC content of the clean data were calculated. All downstream analyses were performed using the high-quality clean data.

The index of the reference genome was built using Bowtie v2.0.6, and single-end clean reads were aligned to the reference genome using TopHat v2.0.9<sup>51</sup>. TopHat was selected as the mapping tool because it generates a splice junction database based on the gene model annotation file and thus produces better mapping results than other non-splice mapping tools.

HTSeq v0.5.4p3 was used to count the number of reads mapped to each gene<sup>52</sup>. Then, the RPKM value of each gene was calculated based on the length of the gene and the read count mapped to it. RPKM (reads per kilobase of exon model per million mapped reads), simultaneously considers the effects of sequencing depth and gene length on the read count, and is currently the most commonly used method for the estimation of gene expression levels<sup>53</sup>.

The differential expression analysis of two groups (three biological replicates per group) was performed using the DESeq R package<sup>54</sup>. The DESeq provides statistical routines for determining differentially expressed genes using a model based on the negative binomial distribution<sup>55</sup>. The resulting P-values were adjusted using the Benjamini and Hochberg's approach for controlling the false discovery rate<sup>56</sup>. Corrected P-values are also called q-values. Genes within a  $|\log_2(\text{fold change})| > 1$  and q-value  $< 0.05$  standard found by DESeq were assigned as differentially expressed.

**Functional analysis of differentially expressed genes.** The GO enrichment analysis of differentially expressed genes was implemented by the GOseq R package<sup>57</sup>. GO terms of differentially expressed genes with q-value  $< 0.05$  were considered significantly enriched terms.

KEGG is a database resource for understanding high-level functions and uses of the biological system (<http://www.genome.jp/kegg/>). The KOBAS software was used to test the statistical enrichment of differentially expressed genes in the KEGG pathways<sup>58</sup>.

**Quantitative real-time PCR validation.** The validation was performed by using RNA from the same sample of DGE sequencing. Quantitative real-time PCR (qRT-PCR) was performed on randomly selected differentially expressed genes. Primer sequences were designed using NCBI primer designing tool (<http://www.ncbi.nlm.nih.gov/tools/primer-blast/>) and synthesized by Invitrogen (Thermo Fisher Scientific Inc., Shanghai, China). cDNA was synthesized with Reverse Transcriptase M-MLV (RNase H-) (TaKaRa) using the oligo dT primer. qRT-PCR with the Power SYBR®Green PCR Master Mix (Applied Biosystems) was carried out on a Multiple Real-Time PCR System (Bio-Rad, America). Each sample was analyzed in triplicate and the expression of the target genes were standardized by the endogenous housekeeping gene (GAPDH). The reaction protocol comprised one cycle of 95 °C for 1 min, forty cycles of 95 °C for 15 s, 63 °C for 25 s. The gene expression was calculated by using the comparative ( $2^{-\Delta\Delta C_t}$ ) method<sup>59</sup>.

**Statistical analysis.** All results are expressed as mean ±

20. Mackenzie, E. L., Iwasaki, K. & Tsuji, Y. Intracellular iron transport and storage: from molecular mechanisms to health implications. *Antioxid Redox Signal* **10**(6), 997–1030 (2008).
21. Pantopoulos, K., Porwal, S. K., Tartakoff, A. & Devireddy, L. Mechanisms of mammalian iron homeostasis. *Biochemistry* **51**(29), 5705–5724 (2012).
22. Robles, J. A. *et al.* Efficient experimental design and analysis strategies for the detection of differential expression using RNA-Sequencing. *BMC genomics* **13**(1), 484 (2012).
23. Xiao, C. *et al.* Effects of a Tripeptide Iron on Iron-Deficiency Anemia in Rats. *Biol Trace Elem* **16**(2), 211–217 (2016).
24. Zhang, Y. *et al.* Effects of ferrous carbamoyl glycine on iron state and absorption in an iron-deficient rat model. *Genes Nutr* **10**(6), 1–8 (2015).
25. Sánchez-Rivera, L., Martínez-Maqueda, D., Cruz-Huerta, E., Miralles, B. & Recio, I. Peptidomics for discovery, bioavailability and monitoring of dairy bioactive peptides. *Food Rev Int* **63**, 170–181 (2014).
26. Krayenbuehl, P. A., Battegay, E., Breymann, C., Furrer, J. & Schulthess, G. Intravenous iron for the treatment of fatigue in nonanemic, premenopausal women with low serum ferritin concentration. *Blood* **118**(12), 3222–3227 (2011).
27. Bailey, J. D., Ansotegui, R. P., Paterson, J. A., Swenson, C. K. & Johnson, A. B. Effects of supplementing combinations of inorganic and complexed copper on performance and liver mineral status of beef heifers consuming antagonists. *J Anim Sci* **79**(11), 2926–2934 (2001).
28. Wang, F. R. *et al.* Effectiveness of treatment of iron deficiency anemia in rats with squid ink melanin–Fe. *Food Funct* **5**(1), 123–128 (2014).
29. Drummond, G. S. & Kappas, A. Prevention of neonatal hyperbilirubinemia by tin protoporphyrin IX, a potent competitive inhibitor of heme oxidation. *Proc Natl Acad Sci* **78**(10), 6466–6470 (1981).
30. Vaghe, N. *et al.* Iron absorption from concentrated hemoglobin hydrolysate by rat. *J Nutr Biochem* **16**(6), 347–352 (2005).
31. Fillebeek, C. *et al.* Mice are poor heme absorbers and do not require intestinal Hmox1 for dietary heme iron assimilation. *Haematologica* **100**(9), e334 (2015).
32. Hamza, I. & Dailey, H. A. One ring to rule them all: tracking of heme and heme synthesis intermediates in the metazoans. *Biochim Biophys Acta-Mol Cell Bios* **1823**(9), 1617–1632 (2012).
33. Orihuela, R. *et al.* Ferritin and metallothionein: dangerous liaisons. *Chem Commun* **47**(44), 12155–12157 (2011).
34. Collins, J. F., Franck, C. A., Kowdley, K. V. & Ghishan, F. K. Identification of differentially expressed genes in response to dietary iron deprivation in rat duodenum. *Am J Physiol-Gastrointest Liver Physiol* **288**(5), G964–G971 (2005).
35. Zhang, G. *et al.* Integrated analysis of mRNA-seq and miRNA-seq in the liver of *Peltobagrus vachelli* in response to hypoxia. *Sci Rep* **6** (2016).
36. Davis, M. R. *et al.* Enhanced expression of lipogenic genes may contribute to hyperglycemia and alterations in plasma lipids in response to dietary iron deficiency. *Genes Nutr* **7**(3), 415–425 (2012).
37. Higgins, C. F. ABC transporters: from microorganisms to man. *Annu Rev Cell Biol* **8**(1), 67–113 (1992).
38. Tomii, K. & Kanehisa, M. A comparative analysis of ABC transporters in complete microbial genomes. *Genome Res* **8**(10), 1048–1059 (1998).
39. Braun, V. & Hantke, K. Recent insights into iron import by bacteria. *Curr Opin Chem Biol* **15**(2), 328–334 (2011).
40. McKie, A. T. The role of Dcytb in iron metabolism: an update. *Biochem Soc Trans* **36**(6), 1239–1241 (2008).
41. Wang, J. & Pantopoulos, K. Regulation of cellular iron metabolism. *Biochem J* **434**(3), 365–381 (2011).
42. Hentze, M. W., Muckenthaler, M. U., Galy, B. & Camaschella, C. Two to tango: regulation of Mammalian iron metabolism. *Cell* **142**(1), 24–38 (2010).
43. Abboud, S. & Haile, D. J. A novel mammalian iron-regulated protein involved in intracellular iron metabolism. *J Biol Chem* **275**(26), 19906–19912 (2000).
44. Zhuo, Z. The differential effects of ferrous glycine chelate and ferrous sulfate to intestinal porcine epithelial cells. In *2016 Joint Annual Meeting Asas* (2016).
45. Ayicicek, A. *et al.* Ferrous sulfate ( $\text{Fe}^{2+}$ ) had a faster effect than did ferric polymaltose ( $\text{Fe}^{3+}$ ) on increased oxidant status in children with iron-deficiency anemia. *Int J Pediatr Hematol-Oncol* **36**(1), 57–61 (2014).
46. Klöpfel, K., Schmid, P., Wuillemin, W. A. & Rüfer, A. Reference values for oral iron absorption of bivalent iron in healthy volunteers. *Swiss Med Wkly* **145**, w14063 (2015).
47. Mazariegas, D. I., Pizarro, F., Olivares, M., Nuñez, M. T. & Arredondo, M. The mechanisms for regulating absorption of Fe bis-glycine chelate and Fe-ascorbate in caco-2 cells are similar. *The Journal of nutrition* **134**(2), 395 (2004).
48. Yeung, C. K., Glahn, R. P. & Miller, D. D. Inhibition of iron uptake from iron salts and chelates by divalent metal cations in intestinal epithelial cells. *J Agr Food Chem* **53**(1), 132–136 (2005).
49. Michelotti, G. A. *et al.* Smoothened is a master regulator of adult liver repair. *J Clin Invest* **123**(6), 2380 (2013).
50. Anders, S. & Huber, W. Differential expression analysis for sequence count data. *Genome Biol* **11**(10), R106 (2010).
51. Trapnell, C., Pachter, L. & Salzberg, S. L. TopHat: discovering splice junctions with RNA-Seq. *Bioinformatics* **25**(9), 1105–1111 (2009).
52. Anders, S. HTSeq: Analysing high-throughput sequencing data with Python. <http://www-huber.embl.de/users/anders/HTSeq/doc/overview.html> (2010).
53. Mortazavi, A., Williams, B. A., McCue, K., Schaefer, L. & Wold, B. Mapping and quantifying mammalian transcriptomes by RNA-Seq. *Nat methods* **5**(7), 621–628 (2008).
54. Robinson, M. D., McCarthy, D. J. & Smyth, G. K. edgeR: a Bioconductor package for differential expression analysis of digital gene expression data. *Bioinformatics* **26**(1), 139–140 (2010).
55. Anders, S. & Huber, W. *Differential expression of RNA-Seq data at the gene level—the DESeq package*. Heidelberg, Germany: European Molecular Biology Laboratory (EMBL) (2012).
56. Benjamini, Y. & Hochberg, Y. Controlling the false discovery rate: a practical and powerful approach to multiple testing. *J Roy Stat Soc B* **289**–300 (1995).
57. Young, M. D., Wakefield, M. J., Smyth, G. K. & Oshlack, A. Method Gene ontology analysis for RNA-seq: accounting for selection bias. *Genome Biol* **11**, R14 (2010).
58. Mao, X., Cai, T., Olyarchuk, J. G. & Wei, L. Automated genome annotation and pathway identification using the KEGG Orthology (KO) as a controlled vocabulary. *Bioinformatics* **21**(19), 3787–3793 (2005).
59. Livak, K. J. & Schmittgen, T. D. Analysis of relative gene expression data using real-time quantitative PCR and the  $2^{-\Delta\Delta CT}$  method. *Methods* **25**(4), 402–408 (2001).

## Acknowledgements

This research was financially supported by the National Natural Sciences Foundation of China (No. 31472102) and the National Key R & D Program (Grant No. 2016YFD0501201).

## Author Contributions

Zhao Zhuo and Jie Feng conceived and designed the experiment. Zhao Zhuo, Shenglin Fang, Qiaoling Hu, and Danping Huang performed the experiment. Shenglin Fang and Qiaoling Hu analyzed the data. Zhao Zhuo wrote the paper. All authors read and approved the final manuscript.

## Additional Information

Supplementary information accompanies this paper at <http://www.nature.com/srep>

**Competing financial interests:** The authors declare no competing financial interests.

**How to cite this article:** Zhuo, Z. et al. Digital gene expression profiling analysis of duodenum transcriptomes in SD rats administered ferrous sulfate or ferrous glycine chelate by gavage. *Sci. Rep.* **6**, 37923; doi: 10.1038/srep37923 (2016).

**Publisher's note:** Springer Nature remains neutral with regard to jurisdictional claims in published maps and institutional affiliations.



This work is licensed under a Creative Commons Attribution 4.0 International License. The images or other third party material in this article are included in the article's Creative Commons license, unless indicated otherwise in the credit line; if the material is not included under the Creative Commons license, users will need to obtain permission from the license holder to reproduce the material. To view a copy of this license, visit <http://creativecommons.org/licenses/by/4.0/>

© The Author(s) 2016